Synthesis of MoS$_2$ nanoparticle deposited graphene/mesoporous MnO$_x$ nanocomposite for high performance super capacitor application

R. Jothi Ramalingam [a,*], Niketha Konikkara [b], Hamad Al-Lohedan [a], Dhaifallah M. Al-dhayan [a], L. John Kennedy [b], S.K. Khadheer Basha [c], Shaban R.M. Sayed [a,d]

[a] Chemistry Department, College of Science, King Saud University, Riyadh, 11451, Saudi Arabia
[b] School of Advanced Sciences, VIT University, Chennai campus, Chennai, 600127, India
[c] Department of Physics, VIT - AP University, Amaravati, 522 501, India
[d] E.M Unit, College of Science, King Saud University, Saudi Arabia

ARTICLE INFO

ABSTRACT

The present study deal with the fabrication of low cost nanocomposite based electrodes based on Nickel foam binder free substrate for supercapacitor applications. The composition of nanocomposite is molybdenum sulphide nanoparticle/graphene coated on mesoporous manganese oxide. The first step is to involve the preparation of mesoporous manganese oxide by non-ionic surfactant assisted method. In the second stage is to deposit the reduced graphene on mesoporous manganese oxide in the presence of ultrasonic irradiation followed by addition of known quantity of commercial MoS$_2$ nanopowder (particle size below 90 nm). The manganese oxide based nanocomposite is showing porous architecture with graphene sheet formation together with MoS$_2$ nanoparticle deposition. N$_2$ adsorption-desorption Isotherm curves for MoS$_2$ nanoparticle (NP) modified graphene oxide/meso-MnO$_2$ and pure meso-MnO$_2$ displayed type IV isotherm with improved surface area values. The reduced graphene oxide (graphene) and MoS$_2$ exist in the form of glassy flaky morphology as well as tubular/needle shapes are obtained after the deposition process in the final nanocomposite. The orderly arranged and anchored nano-sized mesoporous manganese oxide nanocomposites are showed increased specific capacitance (up to 527, 727 and 1160 F/g) and continuous cyclic stability.

Introduction

Pseudo-capacitor based metal oxide based nanocomposites are used to fabricate porous structure nanocomposite deposited carbon materials for conductive and pseudo-capacitor applications. Design the surfaces of conductive materials with pseudo capacitor materials such as RuO$_2$, IrO$_2$, NiO, Co$_3$O$_4$, and conducting polymers, enhances their electrochemical performance by altering the redox properties

[1—5,15]. Compared to other electro catalyst and related pseudo capacitor materials, MnO_2 is a promising electrode material in terms of cost and pollution free as well as easy to prepare in large scale. The big advantage of using manganese oxide is having high theoretical specific capacitance (~1100 F g^{-1}) [6—9]. The different oxidation states of manganese (Mn) ions are main cause for their wide variety of electrochemical applications [8,9]. One of the most practical approaches to improve the usage of manganese oxide involves utilization of large-surface area nanocarbon-based materials, such as single and multi walled carbon nanotubes and graphene like materials to support on manganese oxide and increase its electrochemical activity [10—15]. Graphene, reduced graphene oxides are exhibit effective chemical stability, high electrical conductivity, as well as excellent mechanical properties that are comparable with or even better than carbon nanotubes [16,17]. In reality, improved surface area and conductive supports not only improve the electrical conductivity of MnO_2-based electrodes but also increase their surface activity and it promotes electron transfer. The ions in the manganese oxide lattice has also involve in transport process. The orderly arranged and tightly anchored nano-size MnOx on graphene has also shows enhanced specific capacitance up to 365 F/g and continuous cyclic stability [18—21]. The manganese oxide particles that were mixed and deposited on the surface of graphene contribute increase in the porosity and enhanced specific capacitance. Hence, the power and energy densities of graphene-based devices are much higher than that of MnO_2 nanorod/graphene composites [22]. To improve further the capacitive performance of nanocomposite based super-capacitor device fabrication, some investigations have been focused on increasing their conductivity and capacitance by incorporate or deposit a metal nanoparticle. Li and co-workers demonstrated the fabrication of a novel flexible nano-architecture by coating ultrathin MnO_2 films on highly electrically conductive Zn_2SnO_4 nanowires grown radially on carbon microfibers and it shows the good result, such as specific capacitance of 642.4 F/g (with respect to pristine MnO_2) was achieved in 1 M Na_2SO_4 aqueous solution [23]. The above increased performance is attributable to the formation of ideal electron pathways for the rapid charge—discharge reaction in the presence of highly conductive hollow Ni dendrites. Graphene like other two dimensional nanosheets, such as layered metal dichalcogenides, have also attracted extensive research efforts [24]. MoS_2 has a layered structure consisting of three covalently bonded atomic sandwiches like 35 layer of S—Mo—S [25]. However, the capacitive performance of such composites depends strongly on changes in the local electronic and chemical environments of the active element during the electrochemical charge/discharge process. Noble metal ion incorporated (Au and Pt) in MnOx ternary catalyst is recently utilized as anode catalyst in formic acid fuel cell [26]. As a result of using nano-gold and nano MnOx particle in fuel cell application, it shows enhanced efficiency for fuel cell efficiency compared to using Pt/GC electrode. Costa-serra et al. [27], recently reported the cobalt doped birnessite and todorokite like manganese oxide porous tunnel structured materials for production of hydrogen by steam reforming of ethanol. The steam reforming in catalytic fixed bed reactor results in high selectivity (70—100%) towards hydrogen

production. Sami Ullah et al. [28] reported the study of hydrogen uptake by manganese oxide deposited on multi-walled carbon nanotube composite catalyst by insitu preparation method. Nano MnOx catalyst enhances the hydrogen uptake by hydrogen spillover mechanism using catalyst nanoparticle. From the above recently reported study shows clearly the importance of adding nanoparticle doped MnOx is playing the important catalytic role in enhancing the reaction and improves the efficiency of the electrode materials. The main objective of the present work is to develop highly active modified Nickel foam based electrodes for supercapacitor applications based on non-toxic MnOx based nanocomposite Nickel foam. In the present work, mesoporous manganese oxide is first synthesized by non-ionic surfactant assisted method. The mesoporous MnO_2 is further mixed with graphene oxide to prepare the r-GO (reduced graphene oxide or graphene on MnOx. Then the known quantity of MoS_2 nanoparticle is further added with above prepared nanocomposite to make final form of modified nanocomposite. The porosity structure morphology, and other physico-chemical characterization of the prepared nanocomposite materials have been studied. The as prepared nanocomposite is pressed on nafion substrate to prepare the modified electrode for characterize the electrochemical property to study the specific capacitance.

Materials and method

Sulphuric acid and potassium iodide were bought from Merck India. Nafion perfluorinated resin solution used for working electrode preparation was obtained from Sigma—Aldrich. All the reagents used in the process were of analytical grades. Nickel foam (width: 5 cm, pore number: 110 PPI, Thickness: 1.5 ± 0.5 mm, Density: 480 ± 30 g/m^2) used as substrate were obtained from Winfay Group Company Limited, Shanghai, China. All essential chemicals (manganese sulphate, ammonium persulphate, and alkali), Molybdenum sulphide nanopowder (particle size of 90 nm) and graphene oxide suspension (1000 ppm) are obtained from Sigma Aldrich and used without further purification. X-ray diffraction (XRD) (Miniflex 600), TEM images are recorded at acceleration voltage of 200 kV (JEOL-JEM-2100F, Japan). BET surface area analysis and Nitrogen adsorption desorption analysis carried out using NOVA 2200e (Quantachrome instruments, USA).

Mesoporous manganese oxide is prepared by non-ionic surfactant assisted precipitation method. The synthesized mesoporous MnO_2 is used as a base material to prepare the nanocomposite. Commercially available graphene oxide and MoS_2 nanoparticle (<90 nm) are deposited on as prepared porous MnO_2 to make the nanocomposite. First is to prepare the meso-MnOx is as follow, precipitation was carried out using $MnSO_4$, TritonX-100 as a non-ionic surfactant, ammonium persulphate $(NH_4S_2O_8)$ as the oxidizing agent, and ammonia as directing agent. In the First step, 2 mL of Triton X-100 was dissolved in a minimum amount of deionized water (240 mL) and stirred continuously for 60 min, followed by the addition of 50 mL of 0.1 M $MnSO_4$ dissolved in deionized water. Then, 50 mL of 0.1 M $NH_4S_2O_8$ was added to $MnSO_4$ solution and stirred vigorously for 60 min. After complete mixing,

required quantity of ammonia solution was added drop wise and stirred vigorously until the completion of precipitation. After 12 h of continuous stirring, the solution was filtered and dried at 120 °C to remove volatile impurities. The dried meso-MnO_2 was calcined at 400 °C for 3 h, for complete removal of the surfactant and was used as a support.

Preparation of MoS₂/graphene/meso-MnO₂ nanocomposite

The nanocomposite materials are prepared by ultra-sonication assisted method. Firstly the 100 μL of graphene oxide (GO) suspension (1000 ppm) is mixed with above method prepared 1.0 g of mesoporous manganese oxide (MnOx) in 25 mL of ethanol solution. The above mixed solution ultra-sonicated for 15 min with 20% of amplitude power under ultrasonic irradiation. In the second step, Appropriate amount of MoS_2 added to GO/MnOx. In the present study four different quantity of MoS2 added to the fixed quantity of graphene oxide and meso-MnOx MoS_2 nanopowder was mixed with above prepared suspension of reduced graphene oxide/meso-MnO_2 to make the four types of nanocomposite electrode materials. The above prepared nanocomposite designated as MoSGMn-1, (0.1g MoS_2) MoSGMn-2 (0.075g MoS_2), MoSGMn-3 (0.05g MoS_2), MoSGMn-4 (0.015 MoS_2).

Electrochemical activity and supercapacitor characterization

Electrochemical measurements were carried using a PAR-STAT 4000 electrochemical impedance analyzer in three electrode system. Ag/AgCl and platinum wire was used as the reference and counter electrode respectively. The working electrode is MoS_2/graphene/meso-MnO_2 nanocomposite powder coated over nickel foam substrate. The nickel foam is of length 6 cm and width 1 cm and the area of loading active materials is 1 cm^2 (1 cm × 1 cm). The working electrodes were prepared by mixing MoS_2/graphene/meso-MnO_2 nanocomposite powder 95 wt.% and 5 wt.% nafion to form a paste followed by drying at 80 °C in an oven for 2 h. The mass of the electrode material was found to be approximately 5 mg. The electrolyte was a mixture of 1M H_2SO_4 with 0.5 M KI. Nafion perfluorinated resin solution used for working electrode preparation was obtained from Sigma−Aldrich. All the re-agents used in the process were of analytical grades. Nickel foam (width: 5 cm, pore number: 110 PPI, Thickness: 1.5 ± 0.5 mm, Density: 480 ± 30 g/m^2) used as binder free substrate were obtained from Winfay Group Company Limited, Shanghai, China.

Results and discussion

Powder X-ray diffraction pattern of as prepared samples are shown in Fig. 1. The major intense peaks are indexed and referred with standard powder diffraction data. The as-prepared mesoporous MnO_x matching well with JCPDS file number 24-0508 for the meso-MnO_2 phase of manganese oxide; the d-spacing values and crystalline hkl values are similar to the reported literature values of meso-MnO_2 prepared by other route prepared method. Fig. 1a shows the XRD pattern of as prepared MoSGMn-1 and MoSGMn-3. Fig. 1b shows the comparative XRD images of mesoporous manganese oxide with different phases. In the present method prepared mesoporous MnO_2 based nanocomposite materials are showing mixed mesoporous MnOx contains both MnOx and Mn_2O_3 and the d-space values are matched with XRD phase of reported meso manganese oxide (Fig. 1b) [26]. The pore structure and mesoporous nature of the as prepared MoS_2/graphene/MnO_2 nanocomposites are studied and confirmed by N_2 adsorption-desorption study. Fig. 2(a−d) shows the Transmission electron micrographs of MOSGMn-1, porous
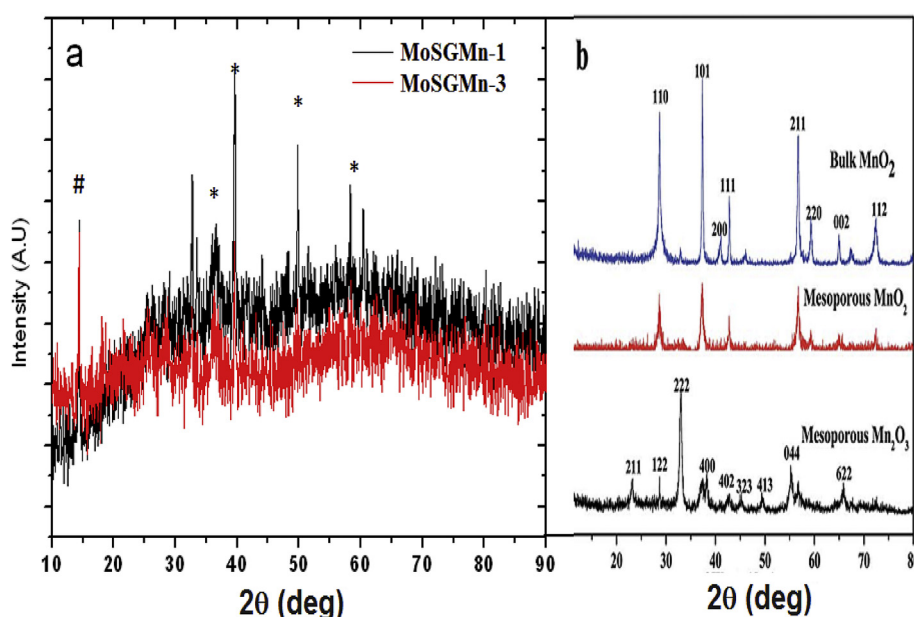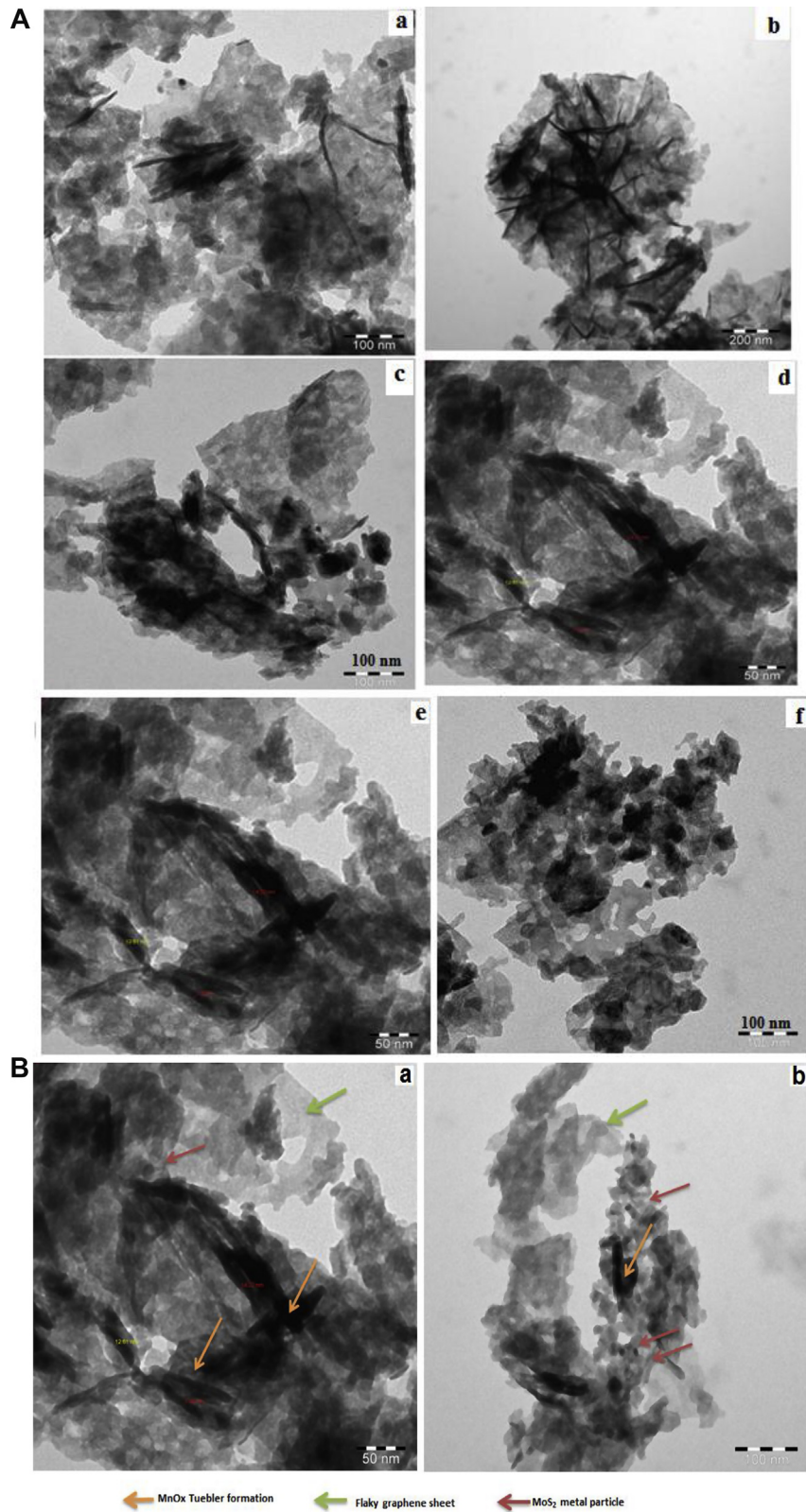

Fig. 1 — X-ray diffraction pattern of (a) MoSGMn-1 (0.1g of MoS₂/GO/meso-MnO₂), MoSGMn-3 (0.05 g of MoS₂/GO/meso-MnO₂) (b) comparative XRD pattern of reported pristine meso-MnO₂ and Mn₂O₃.

Fig. 2 — A (a–d) TEM images of MoS2-GO/meso-MnO$_2$ (MoSGMn-1) at different magnification 2(e–f) TEM images of MoS$_2$-GO/meso-MnO$_2$ (MoSGMn-3) at different magnification. B (a & b) TEM images of MoSGMN-2 at higher magnification (50 nm), the different color arrow mark shows the presence of MoS$_2$ nanoparticle (red arrow) in spherical shape and dark color tubes are belong to MnOx. (For interpretation of the references to color/colour in this figure legend, the reader is referred to the Web version of this article.)
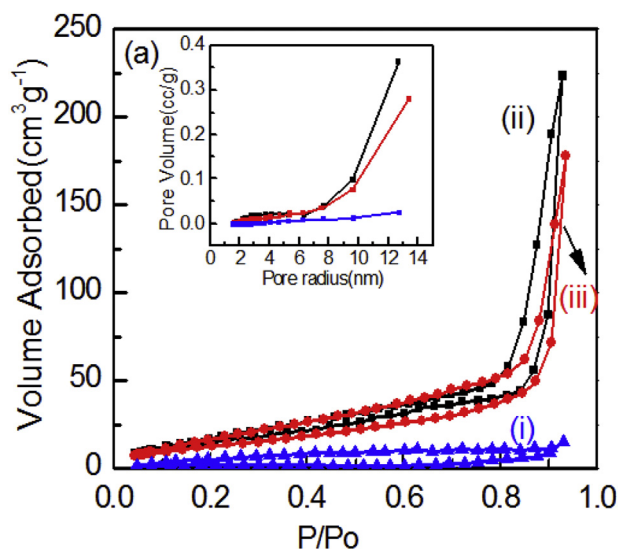
Fig. 3 – N$_2$ adoption-desorption curves for synthesized (i) Bulk MnO$_2$ and (ii) MoSGMn-1 (iii) MoSGMn-2.

manganese oxide exist in the form of aggregated flaky morphology and tubular shape exist due the MnOx, the same kind of tubler structure reported in our previous report of silver doped meso-MnOx catalyst [4]. The addition of GO suspension to meso-MnOx in presence of ethanol and ultrasonic radiation results in the transformation of GO into Graphene, which is clearly shown flashy morphology in the TEM images of Fig. 2A (b&C) and Fig. 2B shown the flaky morphology and MoS$_2$ nanoparticle existence in term of arrow mark {Fig. 2B (a&b)}. The reduced graphene oxide and MoS$_2$ exist in the form of glassy flaky morphology in the final nanocomposite. In some places, the tubular structure of manganese oxide aggregated with reduced graphene oxide and nanoparticle of MoS$_2$ forms the flower shape morphology. Fig. 2e,f shows the TEM images of MoSGMn-3, tubular shape morphology is very visible at 50 nm scale and also nanoparticle deposited on glassy morphology of reduced graphene oxide deposited mesoporous MnO$_2$. Fig. 3 shows the N$_2$ adoption-desorption curves for synthesized meso-MnO$_2$ and MoS$_2$ nanoparticle modified r-GO-meso-MnO$_2$ and their respective pore radius measurement. N$_2$ adsorption-

Fig. 4 – a. Cyclic voltammetry curves for MoSGMn-1 electrode in different scan rates, b. Galvanostatic charge discharge curves for MoSGMn-1 electrode at different current densities, c. Nyquist plot for MoSGMn-1 within the frequency range of 10 MHz to 1 kHz at an AC voltage of 5 mV.
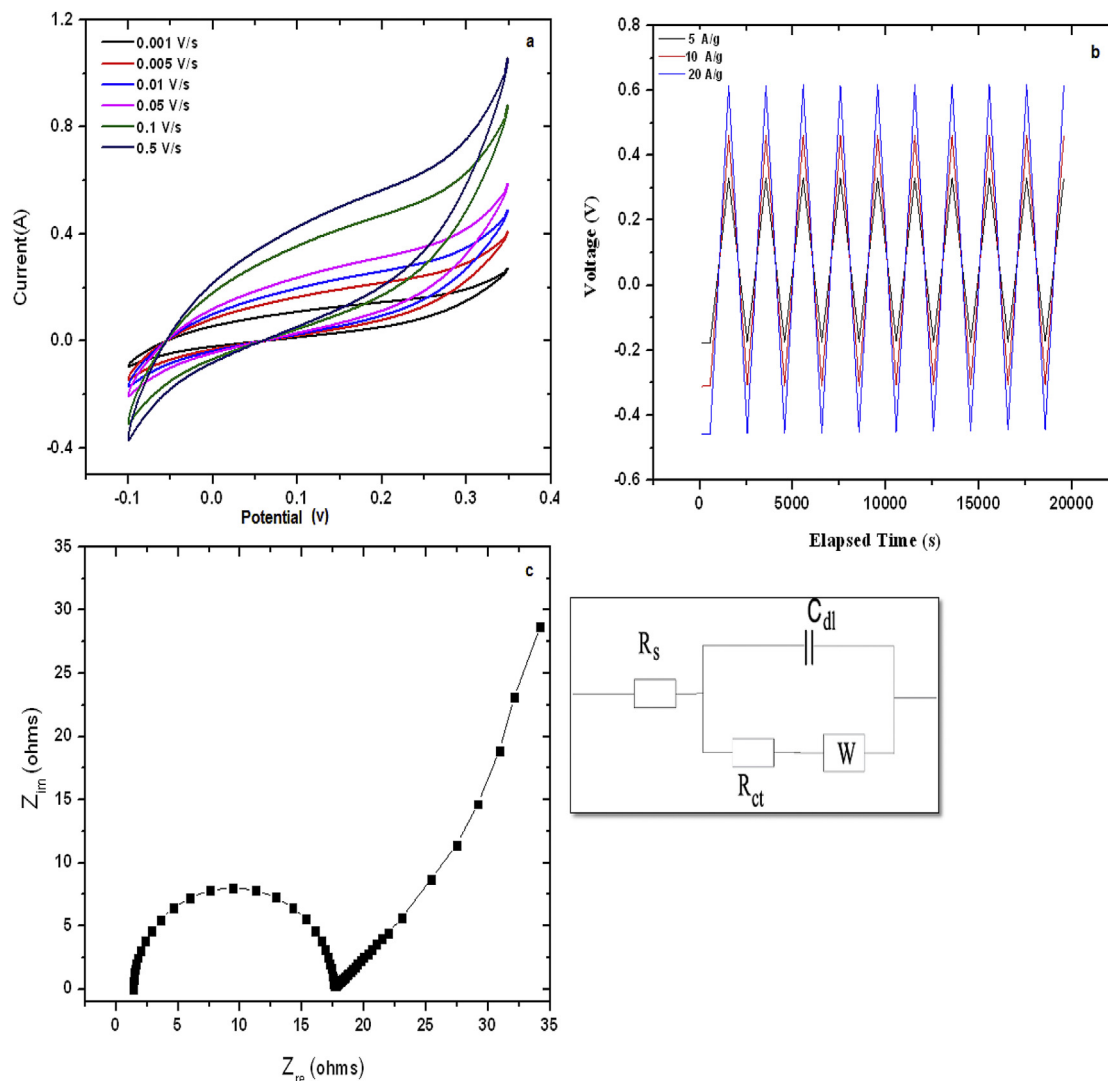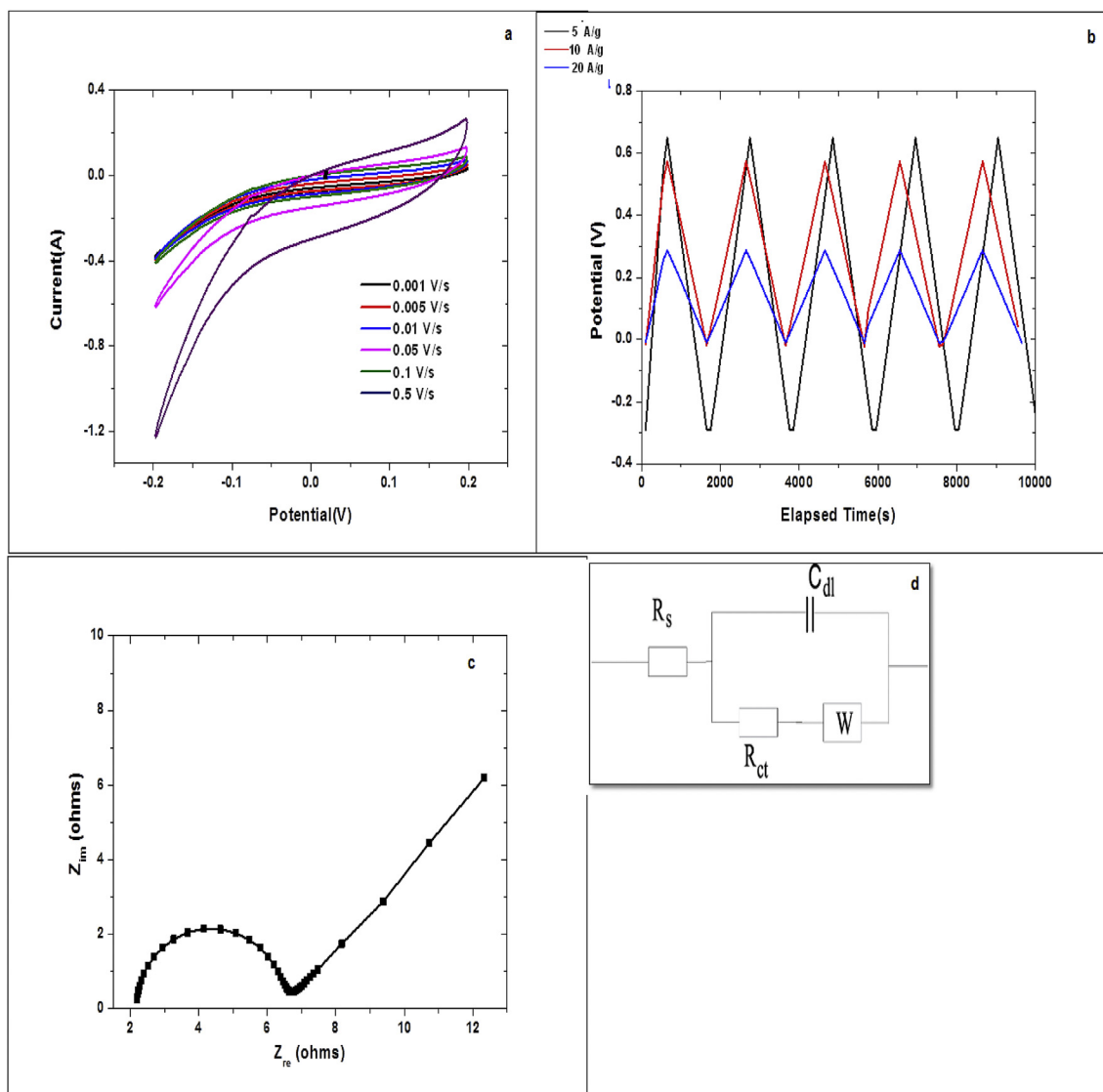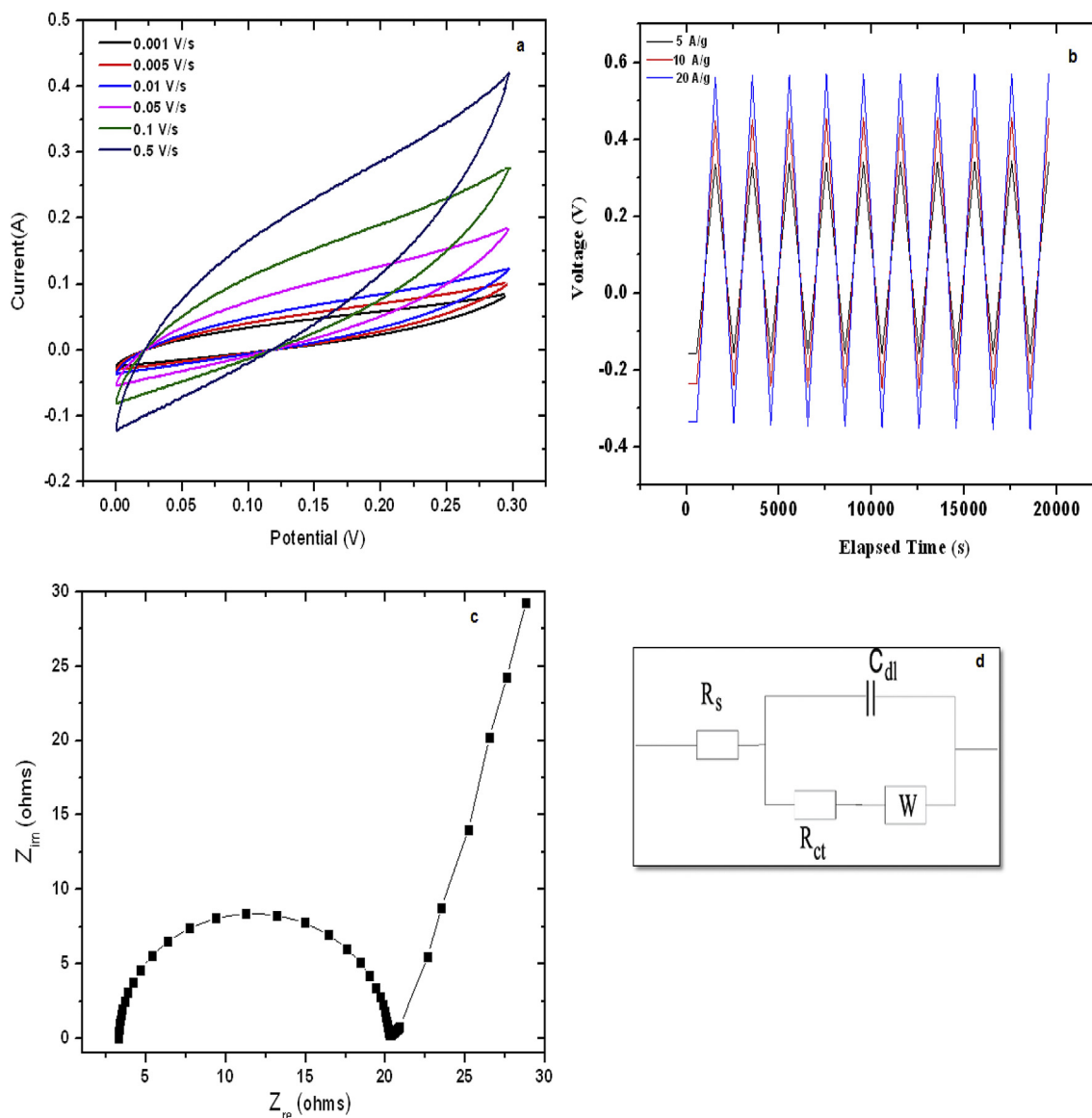
Fig. 5 – a. Cyclic voltammetry curves for MoSGMn-2 electrode in different scan rates, b. Galvanostatic charge discharge curves for MoSGMn-2 electrode at different current densities, c. Nyquist plot for MoSGMn-2 within the frequency range of 10 MHz to 1 kHz at an AC voltage of 5 mV.

desorption Isotherm curves for MoS_2 nanoparticle modified graphene oxide/meso-MnO_2 and pure meso-MnO_2 displayed type IV isotherm, generally Type VI and V type isotherm obtained for mesoporous oxide materials, wherein, the H3 hysteresis loop mostly agreed to the presence of aggregated tubular shaped nanofibers [30]. The BET surface area analysis carried out for meso-MnO_2 and MoSGMn-1 before coating on nickel foam, the surface area of meso-MnO_2 is obtained around 65 m^2/g with pore volume of 3.4×10^{-2} cc/g and in the case of MoSGMn-1 is 56 m^2/g with reduction in pore volume of 2.9×10^{-2} cc/g. N_2-adsorption-desorption curve in Fig. 3 confirms the formation of mesoporous architecture for our method prepared parent meso-MnO_2. In the present method prepared composite electrode materials consist of MoS_2 nanoparticle (less than 2% quantity) with reduced graphene oxide (fixed amount) deposited on meso-MnO_2. In our experiment the different quantity (1–2 wt%) of MoS_2 nanoparticle

deposited on fixed amount of r-Graphene oxide (10 wt%) on meso-MnO_2 (80%). The major compound is meso-MnO_2 for all fabricated Nickel foam electrode for supercapacitor applications. In the present study, we fabricated the working electrode based on Nickel foam coated with active modified above prepared nanocomposite materials and used as modified working electrode for all electrochemical studies and impedance analysis.

Fig. 10A shows the schematic representation Nickel foam based working electrode setup for electrochemical characteristics in the form of half-cell. Fig. 10B shows proposed Nickel foam based electrochemical setup for supercapacitor device fabrication The as prepared 5 mg of active materials is pasted at the one end of Nickel foam shown in drawing and followed by pressed with help of pressing equipment {10 Mp pressure} for 15 s for the purpose of strong physical binding between Nickel foam and prepared nanocomposite.

Fig. 6 – a. Cyclic voltammetry curves for MoSGMn-3 electrode in different scan rates, b. Galvanostatic charge discharge curves for MoSGMn-3 electrode at different current densities, c. Nyquist plot for MoSGMn-3 within the frequency range of 10 MHz to 1 kHz at an AC voltage of 5 mV.

The very less quantity of nafion used to add into active material to make paste for feasible electron transport and good conductivity. After preseing the mixture with Nickel foam forms the strong binding together for electrochemical study.

Nickel foam is commercially available porous conductive and flexible substrate. It's can be used as flexible electrode for device fabrication and easy to replace with the any electrochemical system. Nickel foam has more advantages compared to conventional galssy carbon electrode for electrochemical study includes super capacitor study. Addition of 5 wt% nafion is very small quantity compared to bulk substance (active nanocomposite) and nafion addition due to improves the electron conductivity/feasible the ionic transport in electrochemical process not only for binding to the substrate. Hot pressing procedure is used to bind the active material to the

Nickel foam substrate for easy fabrication of working electrode.

Cyclic voltammetry (CV) technique were used to analyze the electrochemical characteristics of MoS_2/graphene/meso-MnO_2 nanocomposite materials at different scan rates ranging from 1 to 500 mV/s in 1M H_2SO_4 composed with 0.5 M KI as the electrolyte medium (Figs. 4a–7a). In all the scan rates CV curves showed leaf like structure without any redox peaks indicating that electrode material possess good electrical double-layer capacitance [30]. The specific capacitance of the electrode materials is calculated using the following equation and given in Table 1

$$C_{sp} = \frac{1}{vm(V - V_0)} \int_{V_0}^{V} I(V)dV \tag{1}$$
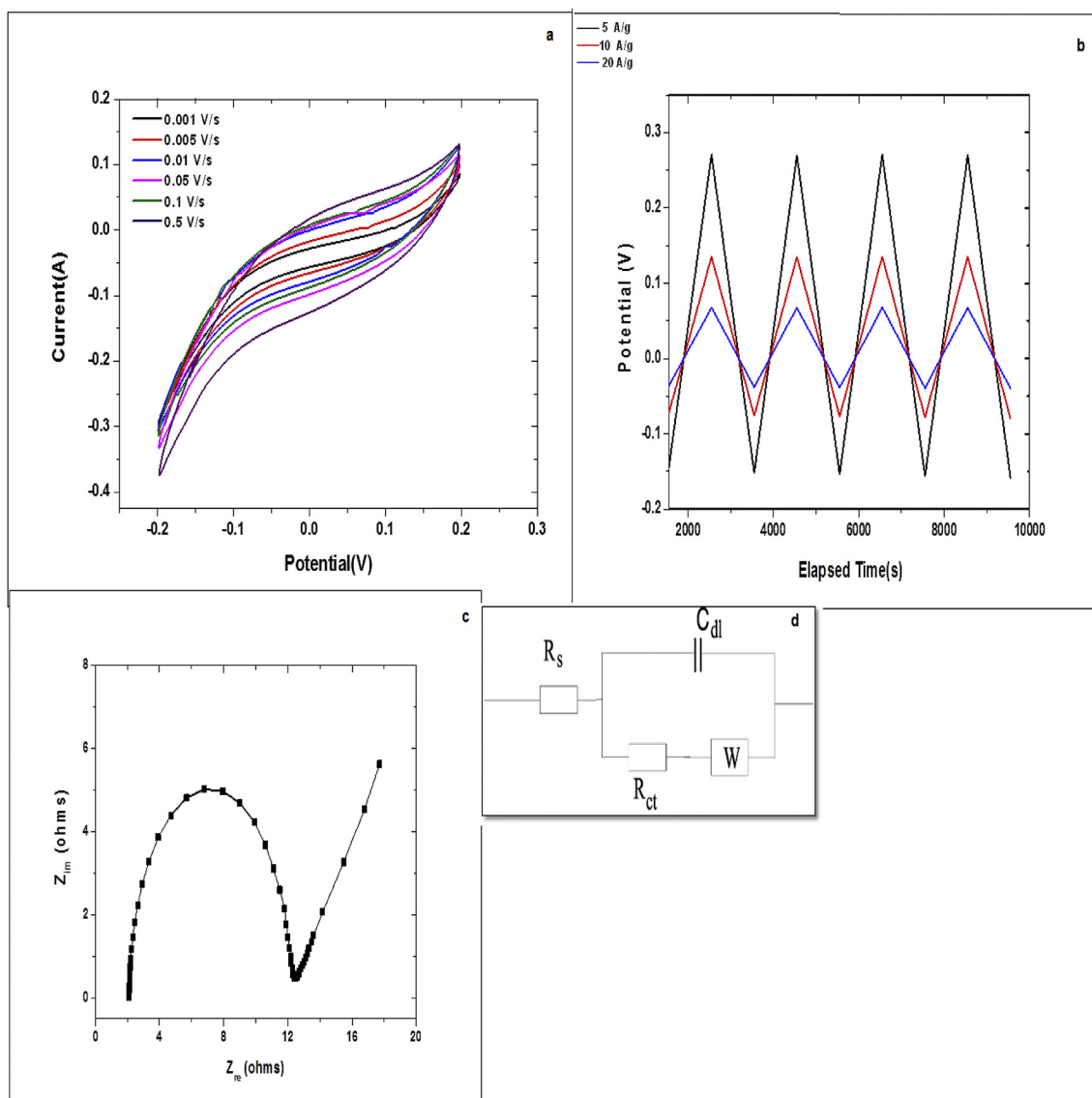
Fig. 7 — a. Cyclic voltammetry curves for MoSGMn-4 electrode in different scan rates, b. Galvanostatic charge discharge curves for MoSGMn-4 electrode at different current densities, c. Nyquist plot for MoSGMn-1 within the frequency range of 10 MHz to 1 kHz at an AC voltage of 5 mV.

where, C_{sp} is the specific capacitance (F/g), is a current response in accordance with the sweep voltage (A), v is the potential scan rate (V/s), V-V_o is the potential window (V) and m is the mass of the electrode in grams [29]. The specific capacitance of MoSGMn-1 to MoSGMn-4 at 1 mV/s is 1160,727,527 and 188 F/g respectively. The higher specific capacitance for MoSGMn-1&2 may be due to three things; (1) From the morphological studies nano needle like structure of the electrode material considerably offer shorter ion diffusion channels during the charging/discharging process [30]. Secondly interconnected structure of the conducting graphene sheets will improve the electron transport over the less conducting MOS_2 and lastly specific surface area provided by mesoporous MnO_2 will be higher in the case of MoSGMn-1 samples. Specific capacitance is decreased with increase in the scan rate in both the samples. At low scan rates ions will get enough time to diffuse into the inner pores of the

electrodes. Consequently more ions are adsorbed on the electrode surface and this leads to better capacitive behavior.

Galvanostatic charge discharge (GCD) measurements at 5, 10 and 20 A/g were performed to verify the super capacitive performance of MoS_2/graphene/meso-MnO_2 nanocomposite materials (Figs. 4b—7b). In the GCD studies symmetrical triangular curve always indicates excellent capacitance behaviors, good electro chemical stability and improved cycle life. From Figs. 6b and 7b; it is clear that both electrodes show excellent charge discharge properties similar to ideal electric double layer capacitor. Cyclic stability is another major factor which defines the performance of a super capacitor. Here both the electrodes exhibited cyclic stability upto 1000 cycles. Specific capacitance values for MoSGMn-1 electrode and MoSGMn-3 electrodes remains 94.7% and 92.6% and respectively, of the initial value even after 1000 cycles (Fig. 8). Columbic efficiency is defined as ratio between charge and
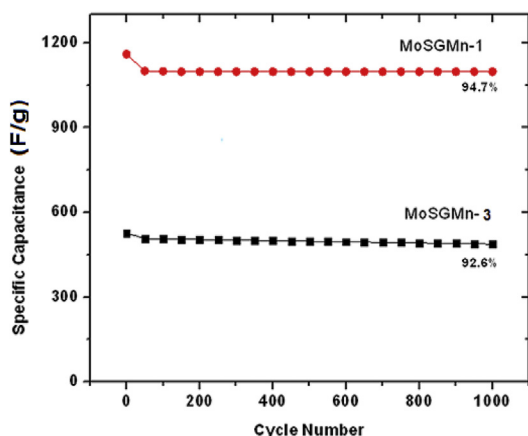
Fig. 8 – Specific capacitance Vs Cycle number for MoSGMn-1 electrode and MoSGMn-2 electrode.

discharge of electron transport with respect to charge/discharge time, in the present method prepared materials is showing Galvano static charge/discharge current is constant upon elapsed time interval for all the four type of nanocomposite electorates (MoSGMn-1 to MoSGMn-4). Even at lower current density, it almost showing above 95% of columbic efficiency and shown in Figs. 4b,6b and7b.

Electrochemical impedance spectroscopies (EIS) were done within the frequency range of 10 mHz to 1 kHz at an AC voltage of 5 mV (Figs. 4c–7c). There are three main regions in the Nyquist plot of MoS_2/r-graphene oxide/meso-MnO_2 nanocomposite electrode. Firstly a large semicircle in the high frequency region which defines the electronic resistance of electrode materials including the solution resistance and charge transfer resistance. The difference of solution resistance and charge transfer resistance will gives equivalent series resistance of the electrode material. Slope of the line creates an angle with the semicircle in the middle frequency region in the Nyquist plot. This region gives us information about the diffusion of electrolyte ions in the pores of the electrode. And the linear line at the low frequency region depicts the capacitive behavior of the MoS_2/graphene/meso-MnO_2 nanocomposite materials. To get more information about the charge transfer mechanism, impedance spectra is fitted into an equivalent circuit (Figs. 4d–7d) and the parameters are given in Table 2. R_s is the solution resistance which contains both ohmic resistance of the electrolyte and also the internal resistance of the electrode materials. Here MoSGMn-1 and MoSGMn-2 electrodes have R_s values 1.48 Ω, 3.28 Ω respectively, which is due to resistance of H_2SO_4-KI electrolyte medium. Lower value of charge transfer resistance (R_{ct}) always paired with better charge discharge performance and also good capacitance. The results obtained in the GCD measurement, matches with good specific capacitance of MoSGMn-2 in cyclic voltammetry studies.

Small contribution of Warburg impedance (W) shows that diffusion of electrolyte ions into the porous network of the electrode materials is superior. Knee frequency is also given in Table 2. It is the maximum frequency at which capacitive behaviors of an electrode material is dominant. Due to low ESR value MoSGMn-2 exhibits higher knee frequency of 109.91 Hz comparing to MoSGMn-1. Table 1 shows the specific capacitance of the different amount of MoS_2 nanoparticle addition on composite of graphene manganese oxide derived from cyclic voltammetry studies. Table 2 explains the impedance analysis values of the modified electrode materials
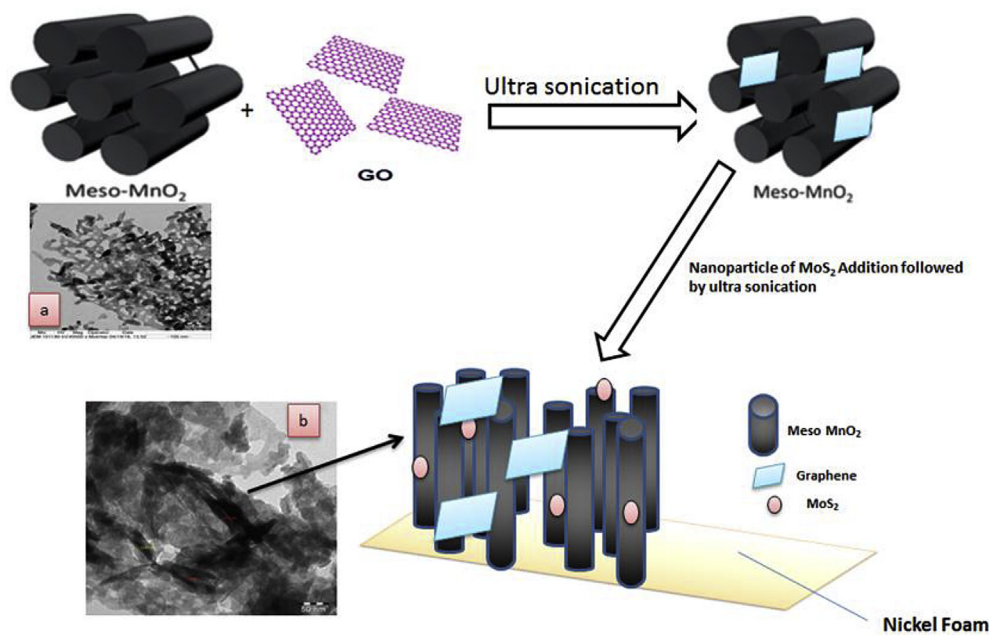
Fig. 9 – Schematic representation of preparation strategy for MoS_2 nanoparticle modified r-Go-meso MnO_2 modified electrode materials coated Nickel foam working electrode for supercapacitor device development inset pictures shows the (a) shows the meso MnO_2 and (b) composite form of meso-MnO_2.
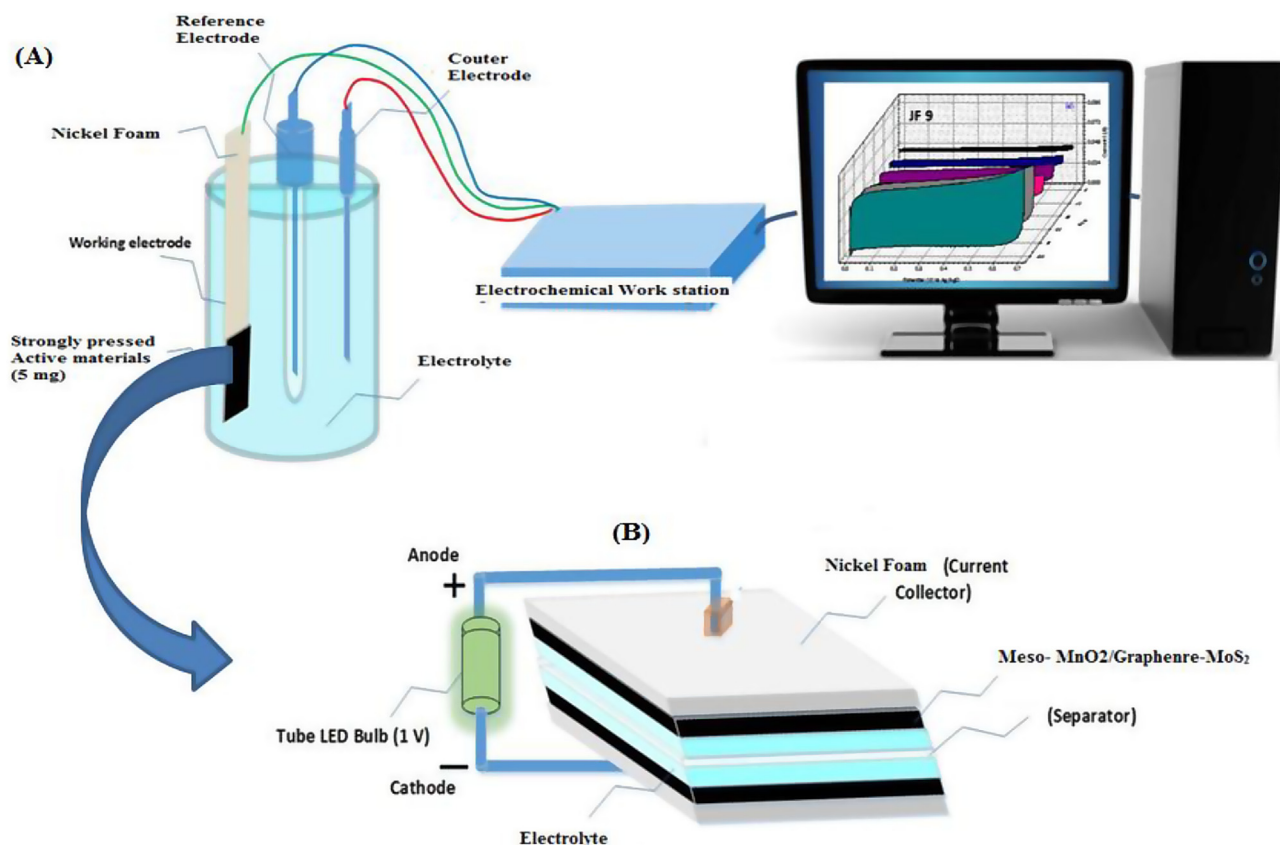
Fig. 10 – (A) Show the schematic representation Nickel foam based working electrode setup for electrochemical characteristics in the form of half cell (B) Proposed Nickel foam based electrochemical setup for Supercapacitor device fabrication.

Table 1 – Specific capacitance (F/g) from CV studies at different scan rates.

Scan rate (V/s)	Specific Capacitance (F/g)			
Sample Code	MoSGMn-4	MoSGMn-3	MoSGMn-2	MoSGMn-1
0.001 V/s	188	527	727	1160
0.005 V/s	35	134	93	520
0.01 V/s	5.80	76	14.8	208
0.05 V/s	9.70	27	5.4	91
0.1 V/s	5.19	17	4.1	50
0.5 V/s	1.37	5	1.63	37

Table 2 – Impedance Spectroscopy and equivalent circuit parameters.

Sample	R_s (Ω)	R_{ct} (Ω)	ESR (Ω)	W (Ω)	Knee frequency f_k (Hz)
MoSGMn-1 (0.10)	3.28	20.82	17.53	8.15	79.43
MoSGMn-2 (0.075)	2.2	6.71	4.51	4.77	25.12
MoSGMn-3 (0.05)	1.40	16.08	14.67	5.65	109.91
MoSGMn-4 (0.015)	2.1	12.40	0.29	1.67	0.316

with respect to the equivalent circuit shown in Figs. 4d–7d. Lower value of charge transfer resistance (R_{ct}) always paired with better charge discharge performance and also good capacitance [31–37]. The schematic representation of modified electrode materials fabrication based on Nickel foam was shown in Fig. 9. The active compound is strongly binded at the one end of Nickel foam. The schematic representation of proposed binder free supercapacitor device fabrication based on modified MoS_2/Graphene/meso-MnO_2 composite shown in Fig. 9a. The method of preparation strategy for modified meso-MnO_2 electrode materials is shown in Fig. 9b.

Fig. 10A shows the half cell and Fig. 10B shows the Nickel foam based flexible supercapacitor device fabrication mechanism with as prepared MnOx based nanocomposite materials. All these electrochemical studies confirm that the optimized loadings between 0.1g top 0.05g of MoS_2 nanoparticle addition on graphene/meso-MnOx nanocomposite materials are excellent electrode materials for high performance supercapacitor device fabrication in terms of enhanced specific capacitance values after the addition of MoS_2 nanoparticle. The different amount of MoS_2 nanoparticle addition from 0.01, 0.05, 0.075 and 0.10 are showing gradual increase in the capacitance values for modified nanocomposite electrode. This unique well-designed binder free Nickel foam based modified meso-MnO_x electrode exhibits a high specific capacitance, good rate capability and

excellent cycling stability for future renewable energy [33,34]. In future study is to exploit the detailed characterization of our route prepared MoS$_2$ nanoparticle added graphene/MnOx composite electrodes by Raman and X-ray photoelectron spectroscopy.

Conclusion

A MoS2/Graphene/MnOx nanocomposite electrode material based on Nickel foam substrate are successfully fabricated by non-conventional method, XRD and BET study confirms the formation mixed phase of MnO2 and Mn2O3 phase with mesoporous architecture. TEM images confirm the aggregated spherical nanoparticle deposition on tubular MnOx with galssy flaky graphene morphology. The higher specific capacitance obtained for MoSGMn-1 and 2 (Tables 1 and 2). MoSGMn-1, MoSGMn-2, MoSGMn-3 and MoSGMn-4 electrodes have R$_s$ values 3.28 Ω, 1.4 Ω, 2.1 Ω and 2.2 Ω respectively which is due to resistance of H$_2$SO$_4$-KI electrolyte medium. Lower value of charge transfer resistance (R$_{ct}$) always paired with better charge discharge performance and also good capacitance. The specific capacitance of the prepared materials studied by CV, GCD and Impendence method and compared together. Here this results matches with good specific capacitance of MoSGMn-1&2 in all studies. Knee frequency is also given in Table 2. It is the maximum frequency at which capacitive behaviors of an electrode material is dominant. Due to low ESR value MoSGMn-3 exhibits higher knee frequency of 109.91 Hz compared to MoSGMn-1&2. All these electrochemical studies confirm that MoS$_2$/graphene/meso-MnO$_x$ nanocomposite materials are excellent electrode materials for high performance supercapacitors fabrication.

Acknowledgement

REFERENCES

[1] Huang M, Li F, Dong F, Zhang Yu X, Li Zhang L. J Mater Chem A 2015;3:21380—423.
[2] Su XH, Yu L, Cheng G, Zhang HH, Sun M, Zhang L, et al. Appl Energy 2014;134:439—45.
[3] Jung KN, Hwang SM, Park MS, Kim KJ, Kim JG, Dou SX, et al. Sci Rep-Uk 2015;5.
[4] Jothi Ramalingam R, Mansoor-Ali Vaali-Mohammed b, Hamad A, Al-Lohedan a, Jimmy Nelson Appaturi. J Mol Liq 2017;243:348—57.
[5] Chen CY, Fan CY, Lee MT, Chang JK. J Mater Chem 2012;22:7697—700.
[6] Wang YX, Xie YB, Sun HQ, Xiao JD, Cao HB, Wang SB. J Hazard Mater 2016;301:56—64.
[7] Wang L, Chua CK, Khezri B, Webster RD, Pumera M. Electrochem Commun 2016;62:17—20.
[8] Shaabani A, Boroujeni MB, Laeini MS. Appl Organomet Chem 2016;30:154—9.
[9] Jiang Y, Jiang ZJ, Chen BH, Jiang ZQ, Cheng S, Rong HB, et al. J Mater Chem A 2016;4:2643—50.
[10] Li R, Hu DP, Zhang SL, Zhang GY, Wang J, Zhong Q. Energy Technol-Ger 2015;3:1183—9.
[11] Zhang Y, Yao QQ, Gao HL, Wang LZ, Jia XL, Zhang AQ, et al. Powder Technol 2014;262:150—5.
[12] Aghazadeh M, Reza Ganjali M, Norouzi P, Sabour B, Emamalizadeh M. Thin Solid Films 2017;634:24—32. https://www.sciencedirect.com/science/article/pii/S0040609017303413.
[13] Huang ML, Huang FF, Yang YC. J Mater Sci Mater Electron 2017;28(15):11192—201.
[14] Cai JW, He MZ, Gu Y, Kang LP, Lei ZB, Yang ZP, et al. Colloid Surface A 2013;429:91—7.
[15] Sui ZY, Wang CY, Shu KW, Yang QS, Ge Y, Wallace GG, et al. J Mater Chem A 2015;3:10403—12.
[16] Su YH, Huang SH, Kung PY, Shen TW, Wang WL. Acs Sustain Chem Eng 2015;3:1965—73.
[17] Liu YS, Li J, Li WZ, Li YM, Chen QY, Liu Y. Int J Hydrogen Energy 2015;40:9225—34.
[18] Liu WW, Lu CX, Wang XL, Tay RY, Tay BK. ACS Nano 2015;9:1528—42.
[19] Li Y, Mei Y, Zhang LQ, Wang JH, Liu AR, Zhang YJ, et al. J Colloid Interface Sci 2015;455:188—93.
[20] Yuan L, Lu Xi-Hong, Xiao X, Zhai Teng, Dai Junjie, Zhang Fengchao, et al. ACS Nano 2012;6:656—61.
[21] Kalubarme RS, Jadhav HS, Park C-J. Electrochim Acta 2013;87:457—65.
[22] Yu Z, et al. Nano Energy 2015;11:611—20.
[23] Bao L, Zang J, Li X. Nano Lett 2011;11:1215—20.
[24] Wang Z, Ma L, Chen W, Huang G, Chen D, Wang L, et al. RSC Adv 2013;3:21675—84.
[25] K. F. Mak, C. Lee, J. Hone, J. Shan and T. F. Heinz, Phys Rev Lett, 105, 136805.
[26] Mohammad Ahmad M, Al-Akraa Islam M, El-Deab Mohamed S. Int J Hydrogen Energy 2018;43:139—49.
[27] Da Costa-Serra JF, Chica A. Int J Hydrogen Energy 2018. Available online 17 January 2018.
[28] Sami Ullah R. Int J Hydrogen Energy 2018. Available online 23 March 2018.
[29] Zhan S, Zhu D, Qiu M, Yu H, Li Y. RSC Adv 2015;5:29353—61.
[30] Said S, Riad M, Helmy M, Mikhail S, Khalil L. Chem Mater Res 2014;6:27—41.
[31] Feng X, Yan Z, Chen N, Zhang Y, Ma Y, Liu X, et al. J Mater Chem A 2013;1:12818—25.
[32] Tang Y, Chen T, Yu S, Qiao Y, Mu S, Zhang S, et al. J Power Sources 2015;295:314—22.
[33] Thangappan R, Kalaiselvam S, Elayaperumal A, Jayavel R, Arivanandhan M, Karthikeyand R, et al. Dalton Trans 2016;45:2637—46.
[34] Wei Suna b, Chen Xuyuan. J Power Sources 2009;193:924—9.
[35] Torabian J, Mahjani MG, Mohammad Shiri H, Ehsani b A, Shabani Shayeh J. RSC Adv 2016;6(47):41045.
[36] Mohammad Shiri Hamid, Ali Ehsani. Bull Chem Soc Jpn 2016;89(10):1201—6.
[37] Naseri M, Fotouhi L, Ali Ehsani, Dehghanpour S. J Colloid interface Sci 2016;484:314.